Article:
Zhang, H, Sun, R, Wu, H et al. (1 more author) (2018) Enhanced photocatalytic activity of wool fibers having titanium dioxide nanoparticles formed inside their cortex. Nanotechnology, 29 (29). 295606. p. 295606. ISSN 0957-4484

https://doi.org/10.1088/1361-6528/aac1b3

Nanotechnology, 29, 295606, Published 18 May 2018, https://doi.org/10.1088/1361-6528/aac1b3

Enhanced photocatalytic activity of wool fibers having titanium dioxide nanoparticles formed inside their cortex

Hui Zhang[*1], Runjun Sun[1], Hailiang Wu[1], and Ningtao Mao[*2]

[1]School of Textile Science and Engineering, Xi'an Polytechnic University, Xi'an 710048, China

[2]School of Design, University of Leeds, Leeds, LS2 9JT, United Kingdom

[*]Email: hzhangw532@xpu.edu.cn (H. Zhang); n.mao@leeds.ac.uk (N. Mao)

Abstract: A wool-TiO_2 nanoparticle composite material having TiO_2 nanoparticles both infiltrated in the matrix between macrofibrils inside cortical cells of wool fibers and grafted on the fiber surface is obtained in this study, and the wool-nanoparticle composite material is found to have highly photocatalytic activities with an extremely narrow band gap of 2.8 eV. The wool fibers are obtained using three successive technical steps: wool fibers are swollen by using lithium bromide, then saturated with tetrabutyl titanate ethanol solution and subsequently treated in boiling water. It was demonstrated that the chemical bonds formed between the as-synthesized TiO_2 nanoparticles and the wool fibers swollen by lithium bromide include C-Ti^{4+}(Ti^{3+}), N-Ti^{4+}(Ti^{3+}), O-Ti^{3+}, and S-Ti^{4+}(Ti^{3+}) bonds. The modified wool fibers have shown markedly improved photocatalytic efficiency due to their enhanced visible light absorption capability, which is much better than the (N-doped) TiO_2 coated wool fibers. In contrast, TiO_2 modified wool fibers swollen by using formic acid have poorer photoactivity, this might be due to the elimination of trivalent titanium between TiO_2 nanoparticles and the wool fibers.

Keywords: Wool fiber, infiltration, TiO_2 nanoparticles, photocatalytic

1. Introduction

Wool fibers have been regarded as a type of miracle fiber for having many unique properties such as three-dimensional crimps, good elasticity, high specific heat coefficient, high moisture absorption capacity and inherent flame retardant properties. Those exceptional properties come from its complex morphology formed by multiple-layered cuticles, composite microstructure of cortex and medulla and chemical compositions of keratin proteins.[1] Modification of its microstructures and chemical composition could lead to wool fibers of novel functionalities. For example, silky Optim wool[2] have been achieved by removal of its exterior hydrophobic cuticles plus stretching slenderization[3] of its hygroscopic interior matrix in cortex; technical keratin protein gels and films have been formed via dissolving wool fibers in reducing agents and ionic liquid.[4] Therefore, new methods to add novel functionalities to wool fibers are always desirable.

Immobilization of a wide variety of catalysts[5] like metal complexes, metal oxides, metallic particles, enzymes, microbes and small organic molecules on various polymers including polyacrylonitrile,[6] polyester,[7] cotton,[8-10] sackcloth,[11] plastic,[12] glass,[13] active carbon[14] and wool fiber is a new technical route to achieve functionalized textile materials. For wool fibers, some of these catalysts (e.g., gold nanoparticles in different sizes) are chemically bonded both onto wool fiber surface and within the wool fiber matrix[15] via potential covalent disulfide bonds, electrovalent forces and salt linkages[16] because wool fibers could provide reactive hydroxyl, carboxyl, amide, and disulfide groups[17] to form cross-links between neighboring polypeptide chains[18] and these catalysts.

Applications of nanoparticle titanium dioxide (TO_2) as one of such catalysts on the surface of keratin wool fibers to provide new functions to wool fibers were widely reported. For example, both of wool fibers coated with pure TiO_2 and N-doped TiO_2 nanoparticles demonstrated excellent photocatalytic properties under visible light.[19] Wool-containing fabrics hydrolyzed with proteases and lipases and then treated with TiO_2 nanoparticles and butane tetracarboxylic acid in an ultrasound bath demonstrated self-cleaning, antibacterial

and UV protection properties.[20] Wool fabrics coated with Ag-doped TiO_2 via in situ photosonochemical synthesis method[21] showed antibacterial/antifungal activities. In addition, anatase TiO_2 nanoparticles were synthesized and immobilized on wool fiber surfaces in a hydrothermal process using tetrabutyl titanate as the precursor,[22] and similar wool fibers of photocatalytic properties were achieved in combination with either chitosan polymers[23] or reactive dyes[24] in one-pot hydrothermal process.

In all of above cases, TiO_2 nanoparticles were formed and grafted only on the surface of wool fibers and these nanoparticles might be washed away or rubbed out during laundering and wear processes, which imposes potential health and safety risks to the users. It would be ideal to infiltrate TiO_2 nanoparticles into the macrofibrils of cortex cells of wool fibers, however, there is no report yet that TiO_2 nanoparticles could be formed inside the cortex of wool keratin fibers. It is also known that the morphology, composition, crystal phase, crystalline size, lattice defect of TiO_2, and different doping elements affect the physiochemical, photocatalytic and antimicrobial properties of TiO_2 nanoparticles,[25] however, it is unclear whether wool-TiO_2 composite structure containing TiO_2 inside its cortical matrix would affect the photocatalytic activity of such wool fibers. In this study, a feasible method to introduce TiO_2 nanoparticles inside the matrix of wool fibers is reported and the photocatalytic properties of resultant TiO_2 modified wool fibers are analyzed.

2. Experimental section

In this research, wool fibers are swollen prior to the diffusion of TiO_2 precursor, then saturated with tetrabutyl titanate solution in ethanol, and subsequently treated with boiling water to form TiO_2 nanoparticles inside wool fibers and onto wool fiber surfaces. Wool materials could be swollen via imbibitional swelling, osmotic swelling and swelling in solutions of neutral salts. Imbibitional swelling results from the absorption of distilled water by wool to form solvates or adsorption compounds; osmotic

swelling in acid or alkaline solutions results from the formation of ionizable protein salts; and swelling in solutions of neutral salts results from the effect of the salts on the cohesion and adhesion forces of the water and the protein.[17] In this study, both formic acid and lithium bromide are used to swell wool fibers. It is known that either formic acid or lithium bromide can swell wool fibers to disrupt inter- and intra-molecular hydrogen bonds existed in wool fibers, but the wool fibers are fully swollen in the formic acid and lithium bromide on the condition including concentrations of swelling agents, temperatures and time duration respectively.

2.1. Materials

80s Merino fine wool fibers of 18.5 microns in diameter from combed tops were obtained from Shandong Nanshan Textile Apparel Co., Ltd. Analytical grade chemical reagents used in the experiment included formic acid (CH_2O_2), lithium bromide (LiBr), tetrabutyl titanate ($Ti(OC_4H_9)_4$), acetone (CH_3COCH_3), ethanol (C_2H_6O), and rhodamine B ($C_{28}H_{31}ClN_2O_3$) dye (or RB dye). The nonionic surfactant AEO-9 ($C_{12}H_{25}O(CH_2CH_2O)_9H$) was purchased from the local market.

2.2. Modification of wool fibers

The wool fibers were treated in the following sequence, and the detailed process route is shown in Figure 1.

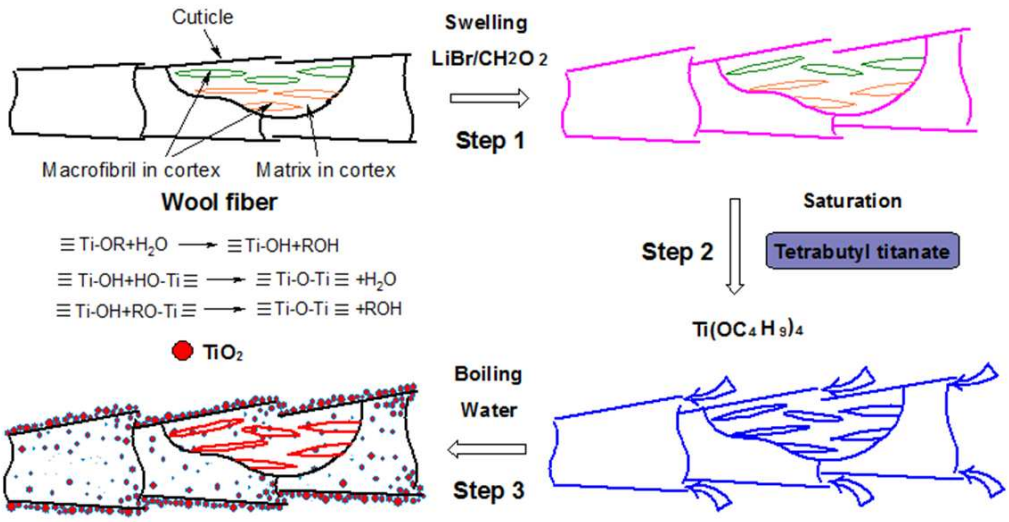

Figure 1. Schematic illustration of the process route of wool fibers

Pretreatment: Wool fibers were washed with 0.1% (w/v) nonionic surfactant AEO-9 at 50°C for 15 min at a liquor ratio of 1:200, then successively immersed in acetone and ethanol solutions at room temperature for 8 min at a liquor ratio of 1:50, and subsequently washed twice with distilled water for 10 min, and finally dried at 50°C for 24 h.

Swelling: There are two schemes to swell wool fibers (see step 1 in Fig. 1), the liquor ratio is kept at 1:200 for both of the two schemes. In scheme one, 0.5 g of pretreated wool fibers was immersed in 100 mL of formic acid aqueous solution in a concentration of 21.2 mol/L at 100°C for 30 min then in 100 mL of formic acid aqueous solution of 26.0 mol/L at room temperature for 20 min to swell wool fibers. During this process, the wool fibers were processed in an ultrasonic oscillator (SY2200-T, Shanghai Shengyuan Supersonic Instrument Equipment Co., Ltd) in a power of 100 W at 55 kHz for 3 min every 10 min. In scheme two, 0.5 g of pretreated wool fibers was immersed into 100 mL of lithium bromide aqueous solution of 2.3 mol/L in concentration at 80°C for 2 h to swell the wool fibers. Then the swollen wool fibers resultant from the two schemes were immersed into 500 mL of distilled water at room temperature for 48 h and this distilled water was replaced by fresh water every 4 hours to remove as much adsorbed swelling agent as possible. Finally, the wool fibers were kept in 100 mL of ethanol solution at room temperature for 48 h before drying.

Treatment of wool saturated with tetrabutyl titanate ethanol solutions: 0.5 g of the swollen wool fibers obtained from both of the two schemes were immersed in 100 mL of tetrabutyl titanate ethanol solution of 0.146 mol/L in concentration at 20°C for 48 hours (step 2 in Fig. 1), assisting with ultrasonic treatment (55 kHz, 100 W) for 20 min every 6 h. The resultant wool fibers were gently treated in 100 mL of distilled water at 100°C for 30 min (step 3 in Fig. 1), then washed successively in acetone, ethanol and distilled water for 10 min respectively, and finally oven dried at 50°C for 24 h. For comparison purposes,

wool fibers without swollen but solely coated with N-doped TiO_2 nanoparticles were also prepared by using hydrothermal method reported in our previous study.[19]

2.3. Characterization and measurement

Wool fibers to be observed in field emission scanning electron microscopy (FESEM), ZEISS EVO18, were sputtered with a thin layer of platinum. The elemental mappings of the cross sections of modified wool fibers were characterised by using energy dispersive X-ray (EDX), Oxford INCA Energy 400 spectroscopy attached to the above FESEM instrument. The cross-sections of wool fibers were obtained by snapping or pulling the wool fibers quenched in liquid nitrogen for 10 min. The distributions of as-synthesized particles in the cross sections of modified wool fibers were analyzed by using transmission electron microscopy (TEM), Hitachi H-600 and JEOL3010, operated at 75 and 200 keV, respectively. Thin specimens of the cross sections of wool fibers of approximately 200 nm in thickness were obtained by microtoming (3501A Richert-jung Ultra Cut E, Reichert, American Instrument) wool fibers embedded in EMbed 812 epoxy resin at room temperature for 2 hours and then cured at 60^{o}C for 48 hours. The chemical groups of wool fibers were characterized using Fourier Transform Infrared (FTIR) spectra (Spotlight 400 & Frontie, PerkinElmer) on the attenuated total refraction (ATR) mode in the wavenumber ranging from 650 to 4000 cm^{-1} at a resolution of 4 cm^{-1}. The chemical bonding states between the as-synthesized particles and wool fibers were investigated by using X-ray photoelectron spectroscopy (XPS), AXISULTRA (Kratos, UK). The XPS spectra were recorded with monochromatic Al Kα (1486.7 eV) line at a power of 100 W (10 mA, 10 kV) with the vacuum about 10^{-8} Torr. The charge neutralizer was employed to compensate surface charge effects, and binding energies were calibrated using the C_{1s} hydrocarbon peak at 284.8 eV. The crystallinity and orientation of wool fibers before and after treatments were measured by a micro X-ray diffraction analysis system, D/MAX-Rapid II (Rigaku, USA), operated at 40 kV and 50 mA with exposure time of 800 s. Based on the Segal's empirical method,[26] the crystallinity index CI (%) of wool fibers was

calculated by the equation (1) below.

$$CI(\%) = \frac{I_9 - I_{14}}{I_9} \times 100\% \quad (1)$$

Where $I_{9°}$ is the peak intensity of the crystalline fraction at 2θ=9° and $I_{14°}$ is the peak intensity of the amorphous fraction at 2θ=14°. Based on the azimuth diffraction pattern of the $I_{9°}$ crystal face, the orientation degree[27] y of protein molecules in wool fibers in the range of 0° to 180° was calculated by the equation (2) below.

$$y = \frac{180^o - HW}{180^o} \quad (2)$$

Where HW is the full width at half maximum of the diffraction peak (FWHM).

The optical properties of wool fibers before and after treatments were determined by using diffuse reflectance spectra (DRS), Lambda 950 (PerkinElmer), in the wavelength range of 200 to 800 nm at a scanning rate of 600 nm/min. As cationic methylene blue (MB) dye could be reduced in a reducing environment to its colourless leuco form which does not absorb visible light[28], and switched back to blue colour in an oxidizing environment[29]; In addition, MB mainly exists as a stable MB@TiO_2 polymeric sol on the surface of TiO_2, TiO_2 colloid hydrosol shows highly selective photocatalysis of MB and other cationic dyes than anionic methyl orange (MO)[30] which can react with proteins such as bovine serum albumin in acid condition[31], thus both MB and MO might give misleading indication if they were used as photocatalytic indicator in this case. In contrast, RB dye can be oxidized by the pathways of N-deethylation, chromophore cleavage and mineralization under visible light[32, 33]. Thus the photocatalytic degradation of resultant wool fibers was demonstrated using the RB dye solution of 2 mg/L in concentration in a photochemical reactor, YM-GHX-V (Shanghai Yuming Instrument Co. Ltd), equipped with a 1000 W of mercury lamp. 0.2 g of the wool fibers was kept in 50 mL of RB dye aqueous solution for 4 hours in a dark place, then the wool fibers in the dye solution were irradiated with UV and visible light irradiations

respectively. Under irradiation of UV light, the UV-passing filter was used to block off visible light. The UV radiation intensities were 23 $\mu W/cm^2$ at 220-275 nm and 4.8 mW/cm^2 at 290-390 nm, measured using ST-512 and TM-213 UV illumination meters respectively. For irradiation of visible light, the UV cut-off filter was used to block off UV light. The intensity of visible light was greater than 2×10^7 lux, measured by using a TES 1332A digital light intensity meter. The absorbance of RB dye solution at the maximum absorption wavelength of 554 nm was measured using a VIS-7220N spectrophotometer (Beijing Rayleigh Analytical Instrument Corp.) at a certain interval of exposure time. The decolorization grade of RB dye solutions, D (%), was calculated by the equation (3) below,

$$D = (1 - C_t / C_0) \times 100\% \quad (3)$$

Where C_0 is the initial concentration of RB aqueous solution; C_t is the concentration of RB solution at time t (minutes). The photocatalytic effect of wool fibers on the decomposition of the RB dyes was represented by the average of the decolorization grade in four tests. The stabilities of the wool fibers obtained from scheme two for photodegradation of the RB dye solution were also conducted over four continuous cycles under UV and visible light irradiation respectively. The wool fibers collected from the RB solution after each photodegradation experiment were washed successively using ethanol and deionized water to remove residual dyes from the wool fibers before oven drying. Furthermore, the existence of Ti element in the finally degraded RB solution was measured using a Sequential Inductively Coupled Plasma Emission Spectrometer (ICP2060T, Skyray Instruments).

3. Results and discussion

3.1. Surface morphology of TiO_2 modified wool fibers

The representative FESEM images of the surface morphologies of modified wool fibers obtained in both schemes one and two are shown in Figure 2. A thick layer of paste-like coating embedded with granular

particles/aggregates is covered on the surfaces of wool fibers. Most of the scales of wool fibers are relatively well remained after being treated with swelling agents and titanate tetrabutyl solutions. It is observed in the high-resolution FESEM images (e.g., Fig. 2 (c) and (f)) that these agglomerated particles have secondary structures and are composed of nanoscale primary particles.

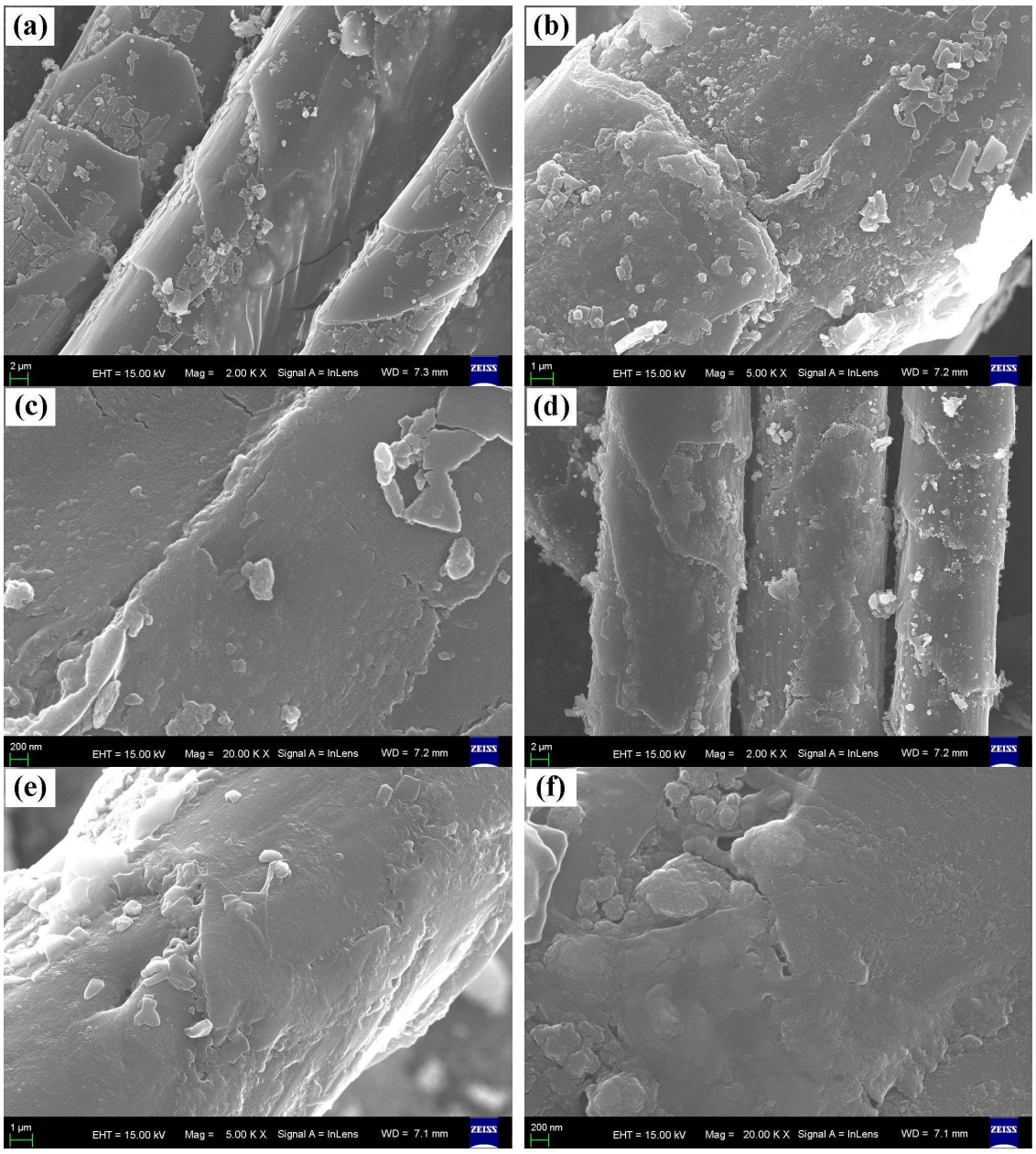

Figure 2. FESEM images of the modified wool fibers: (a), (b) and (c) for scheme one; (d), (e) and (f) for scheme two

3.2. Mapping of chemical element distribution in the cross sections of modified wool fibers

The EDX elemental mappings of the cross sections of modified wool fibers obtained in both of the

schemes are shown in Figure 3. While elements of carbon, nitrogen, oxygen, and sulfur are homogeneously distributed throughout the whole cross sections of wool fibers produced in both schemes, most of the titanium primarily appeared around the edges of the cross-sections of modified wool fibers. It is noticed that a small amount of titanium scattered in the cortex of wool fibers suggesting that the tetrabutyl titanate might penetrate through scales into cortex matrix of the wool fibers. It is also noticed that bromine is detected whereas lithium is not found in the wool fibers swollen in lithium bromide (scheme two). This might be because bromide has formed strong chemical bonds with protein in wool fibers and lithium has been washed away.

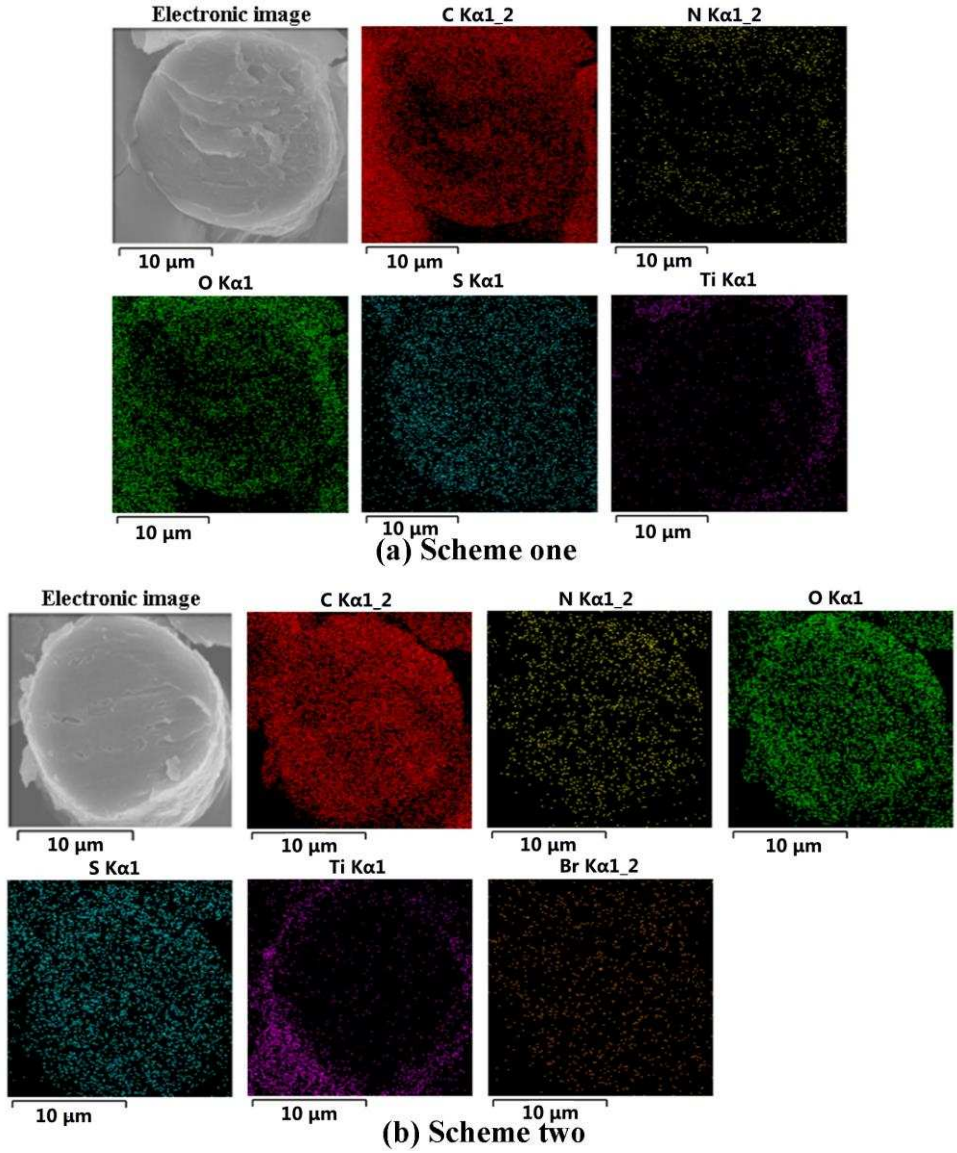

Figure 3. EDX elemental mappings of the cross sections of modified wool fibers: (a) scheme one; (b)

scheme two

3.3. TiO_2 nanoparticles in the cross sections of modified wool fibers

TiO_2 nanoparticles appeared in the cross-section of wool fibers are of the most interests to us and have been further examined using TEM, high-resolution TEM and SAED. The images of the modified wool fibers from TEM, high-resolution TEM images and SAED patterns are shown in Figure 4. It is apparent in the cross-sectional TEM images of modified wool fibers that the surfaces of the wool fibers in both schemes are covered by a layer of TiO_2 granular particles. For wool fibers produced in scheme one, it is confirmed that most of the as-synthesized TiO_2 particles are distributed on the outer border of the cross-section of the fibers, and some of the tetrabutyl titanate solution might have infiltrated through the scale's root into the cortical layer of the modified wool fibers to form TiO_2 particles between cuticles as well as between cuticle and cortex layers. The particle sizes of as-synthesized nano-sized particles are less than 10 nm and the average distance between adjacent lattice planes is measured to be 0.352 nm, as testified by the high-resolution TEM image. The result is consistent with the d-spacing 0.35 nm of the (101) plane of anatase TiO_2.[34] The diffraction rings in the corresponding SAED pattern are ascribed to the lattice planes (101), (004), (200), (105) and (211) of poly-crystalline anatase TiO_2.[35] While a few Ti element underneath the scales of wool fibers was indicated in EDX mapping in section 3.2, we expected a few TiO_2 particles formed in the interior of modified wool fibers to be found in the TEM images of cross-section of wool fibers images. However, there is no such TiO_2 particles found in the cortex of the modified wool fibers in the TEM images as indicated in the EDX mapping. There are a few possible reasons below for this contradiction phenomenon and it is unclear how this happens yet. (1) the titanium element appeared in the cross-section of wool fibers in EDX mapping is due to the contamination of EDX samples, and the Ti element might be due to the falling off of the TiO_2 particles attached on the surface of the wool fibers; (2) the size of the TiO_2 particles formed inside the cortex of the wool fibers is too small which is beyond the

resolution of the TEM; (3) the titanium element is from the residue of tetrabutyl titanate solution infiltrated into wool fibers but there is little (or not any) TiO_2 particles formed inside the wool cortex. Further investigation of these modified fibers is needed. In wool fibers produced in scheme two, the nano-sized TiO_2 particles are found not only in the brim of the cross-section of the wool fibers, but also inside the cortical cells. It is confirmed in the further analysis in corresponding SAED patterns that the agglomerated nanoparticles coated on the fiber surface are poly-crystalline anatase TiO_2 nanoparticles of 10 nm in sizes, and the nanoparticles (or nanoparticle aggregates) formed inside the cortex are noncrystalline and their sizes are about 50-60 nm.

It is known that the sizes of cortical cells are around 2 μm[1] while the noncrystalline TiO_2 nanoparticles scattered randomly inside the cortex in the distances ranging from 50 nm to 500 nm, therefore, these nanoparticles must have formed inside the cortical cells. In addition, it is noticed that the macrofibrils inside the cortical cells are in the size of 200 nm,[1] the gaps between packed macrofibrils are thus at least around 50-70 nm if these macrofibrils are assumed to be circular cylinders and closely stacked together. Therefore, the noncrystalline TiO_2 nanoparticles are likely formed in the gaps between macofibrils. We could almost certainly exclude the possibility of these noncrystalline TiO_2 nanoparticles (or nanoparticle aggregates) of 50-60 nm formed inside macrofibrils, because the size of microfibrils[1] inside the macrofibrils are around 7 nm and the gaps between these microfibrils might be around 1-2 nm which can not accommodate the nanoparticles of 50-60 nm in sizes; if there are any such smaller TiO_2 nanoparticles formed inside macrofibrils, its sizes must be less than 2 nm and observation of those small nanoparticles is beyond the capability of our facilities. In a summary, we can conclude that the noncrystalline TiO_2 nanoparticles in the sizes of 50-60 nm are formed in the gaps between macrofibrils inside cortex cells of wool fibers. This clearly indicates that the tetrabutyl titanate solution has successfully penetrated through the cell membrane complex (CMC) into the cortex of wool fibers via the root of fiber scales and

noncrystalline TiO_2 nanoparticles are formed in the gaps between macrofibrils inside the cortical matrix.

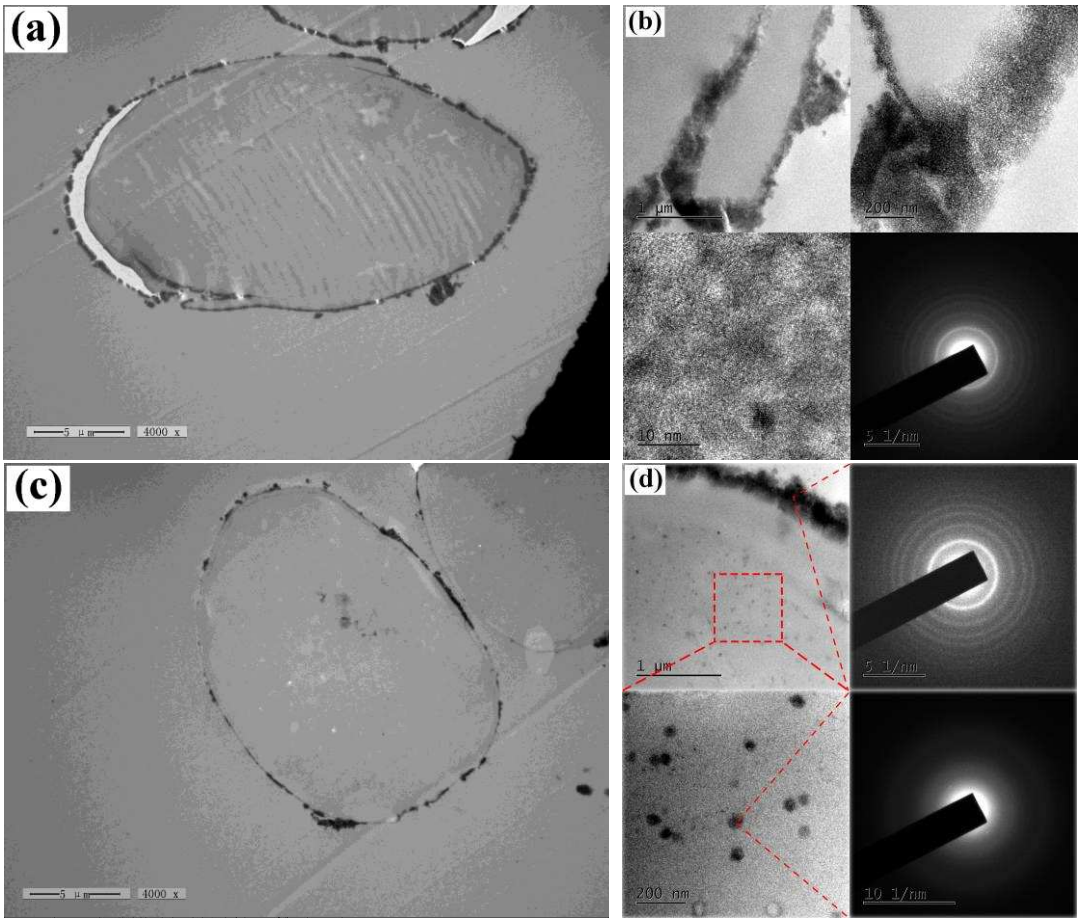

Figure 4. TEM and high-resolution TEM images and SAED patterns of modified wool fibers: (a) and (b) for scheme one; (c) and (d) for scheme two

3.4. Chemical bonding between TiO_2 nanoparticles and wool fibers

The FTIR spectra of wool fibers before and after treatments are shown in Figure 5. It is found that the characteristic absorption peaks of wool fibers have no distinct changes after chemical modifications in both schemes. For wool fibers produced in scheme one, the peaks at 2960 cm^{-1} (CH_3 asymmetric stretching) and 2926 cm^{-1} (CH_2 asymmetric stretching) of the original wool fibers are shifted to 2964 cm^{-1} and 2918 cm^{-1} respectively. At the same time, the peaks at 1074 cm^{-1} and 922 cm^{-1} (C-O stretching) are shifted to 1076 cm^{-1} and 919 cm^{-1} respectively. For wool fibers produced in scheme two, the N-H stretching peak centered at 3280 cm^{-1} of the original wool fibers increases to 3283 cm^{-1}, which is presumedly caused by

the surface absorbed-water resulting from TiO_2 nanoparticles. The CH_3 and CH_2 asymmetric stretching peaks at 2960 cm^{-1} and 2926 cm^{-1} are shifted to 2959 cm^{-1} and 2931 cm^{-1}, respectively. The C-O stretching peak at 922 cm^{-1} decreases to 919 cm^{-1}. The results suggest that the swelling agent and titanate tetrabutyl have little effect on the structure of wool fibers during process. In addition, there is no any new chemical bond found after these chemical modifications of wool fibers. It is thus difficult to conclude from the FTIR spectra whether the as-synthesized TiO_2 nanoparticles are chemically integrated with wool fibers.

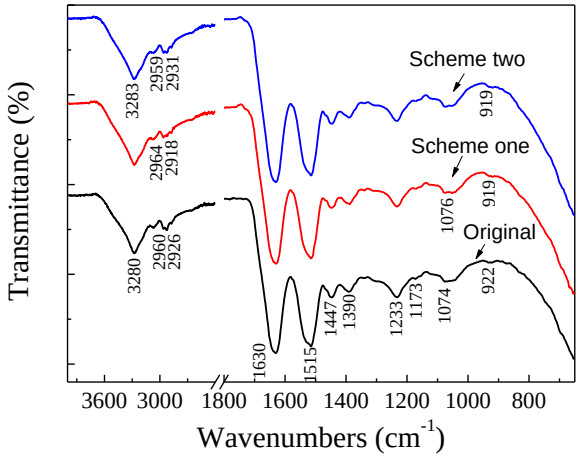

Figure 5. FTIR spectra of wool fibers before and after treatments

To further clarify the chemical bonding states between TiO_2 nanoparticles and wool fibers, the XPS technique is employed and both survey spectra and core level spectra of C_{1s}, N_{1s}, O_{1s}, S_{2p}, and Ti_{2p} of the surface of wool fibers including original wool fibers, modified wool fibers produced in schemes one and two are shown in Figure 6. The results of XPS elemental analysis are summarized in Table 1. Titanium element is detected on the modified wool fibers and the atomic concentrations of Ti are 1.82% and 2.36% for schemes one and two respectively. The changes of C_{1s}, N_{1s}, O_{1s}, and S_{2p} in the survey spectra of original wool fibers and modified wool fibers could indicate the new bonding formed on the modified wools. In comparison with the C_{1s} XPS spectra of the original wool fibers, the subpeaks of C-C/C-H, C-N/C-O, and C=O/C(O)N[36] of modified wool fibers are shifted from 284.78, 286.44, and 288.57 eV to

284.82, 286.35, and 288.47 eV for scheme one and 284.78, 286.07, and 287.33 eV for scheme two, respectively. In addition, one new subpeak at the binding energy of 283.23 eV (C-Ti^{4+}) for scheme one and 283.35 eV (C-Ti^{4+}/Ti^{3+}) for scheme two is observed,[37] which is assigned to C atoms of wool fibers bonded to Ti of TiO_2. Another new subpeak at 289.30 eV (O=C-O)[38] is identified only in scheme two, and this bond might be produced in the hydrolysis of wool fibers swollen by lithium bromide. With regard to the N_{1s} XPS spectra, the subpeak at 399.79 eV (C-N/N-H) for the original wool fibers is separated into two new subpeaks at 398.71 eV (N-Ti^{4+}) and 400.43 eV (C-N/N-H) for scheme one, and three new subpeaks at 398.54 eV (N-Ti^{4+}/Ti^{3+}), 400.43 eV (C-N) and 402.23 eV (N-H) for scheme two respectively,[39] which may be attributed to the N element replacing the O element in the crystal lattice of TiO_2. The O_{1s} peak of the original wool fibers can be deconvoluted into two subpeaks at both 530.20 eV (O=C) and 531.75 eV (O-C).[40] They are shifted to 530.35 and 531.84 eV respectively for the wool fibers from scheme one and to 533.51 and 534.84 eV for the fibers from scheme two. Additionally, it is noticed that two new subpeaks at 528.92 eV (O-Ti^{4+}) and 533.37 eV (chemisorbed -OH groups)[41] are formed in scheme one, while three new subpeaks at 528.85 eV (O-Ti^{3+}), 530.62 eV (O-Ti^{4+}) and 532.02 eV (O=C-O)[42] in scheme two. This indicates that the O atoms of the wool fibers are bonded to Ti of TiO_2 for both schemes. For the S_{2p} XPS spectra, the subpeaks at 163.50 eV (S-S) and 164.92 eV (S-H)[43] of the original wool fibers are shifted to 163.91 and 165.71 eV for scheme one, and to 164.05 and 166.20 eV for scheme two, respectively. Similarly to O_{1s} in the spectra, a new peak at a lower binding energy of 162.48 eV (S-Ti^{4+}) for the fibers in scheme one, and at 162.15 eV (S-Ti^{4+}/Ti^{3+}) for scheme two appears,[44] and this new peak is ascribed to the new bonding formed between S atoms of wool fibers and Ti of TiO_2. The Ti_{2p} XPS spectra of TiO_2 produced in both schemes are in line with the XPS spectra of C_{1s}, N_{1s}, O_{1s}, and S_{2p}. More importantly, while the sub-peaks at 463.99 and 458.34 eV corresponding to C-Ti^{4+}/N-T^{4+}/O-Ti^{4+}/S-$Ti^{4+}{}_{2p1/2}$ and C-Ti^{4+}/N-T^{4+}/O-Ti^{4+}/S-$Ti^{4+}{}_{2p3/2}$[45] respectively appear in the fibers from scheme one, the trivalent titanium

(Ti^{3+}, electron trapping sites) ions are not formed in them. This might be because the H^{+} ions, which are resulted from formic acid adsorbed or absorbed by wool fibers, inhibit the formation of photo-generated electrons, thereby not favoring the reduction of Ti^{4+} to Ti^{3+} ions.[46] On the contrary, the Ti_{2p} peak for the fibers from scheme two is deconvoluted into four subpeaks, the subpeaks at 465.45 and 459.84 eV representing C-Ti^{4+}/N-Ti^{4+}/O-Ti^{4+}/S-$Ti^{4+}{}_{2p1/2}$ and C-Ti^{4+}/N-Ti^{4+}/O-Ti^{4+}/S-$Ti^{4+}{}_{2p3/2}$ respectively, and the subpeaks at 463.37 and 457.36 eV standing for C-Ti^{3+}/N-Ti^{3+}/O-Ti^{3+}/S-$Ti^{3+}{}_{2p1/2}$ and C-Ti^{3+}/N-Ti^{3+}/O-Ti^{3+}/S-$Ti^{3+}{}_{2p3/2}$ respectively.[47] The four subpeaks have confirmed the new bindings of C-Ti^{4+}(Ti^{3+}), N-Ti^{4+}(Ti^{3+}), O-Ti^{3+}, and S-Ti^{4+}(Ti^{3+}) being formed in the lattice of TiO_2 crystal produced in scheme two, suggesting these crystallized TiO_2 nanoparticles are chemically bonded with wool fibers.

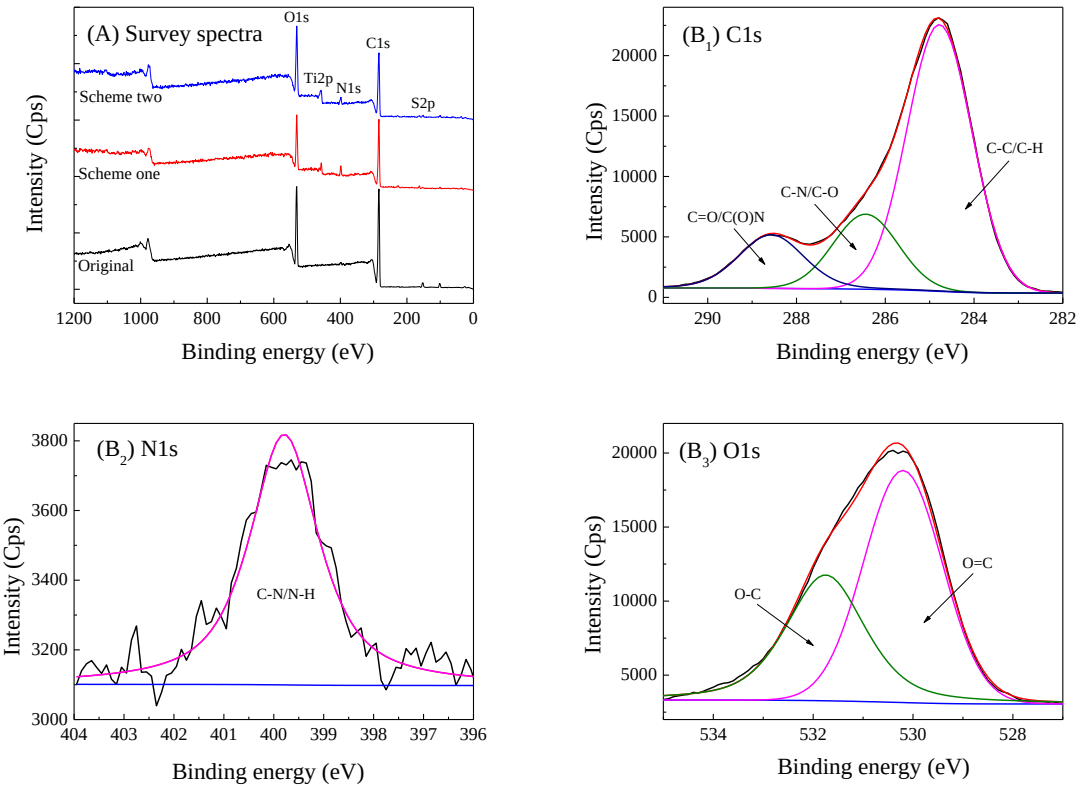

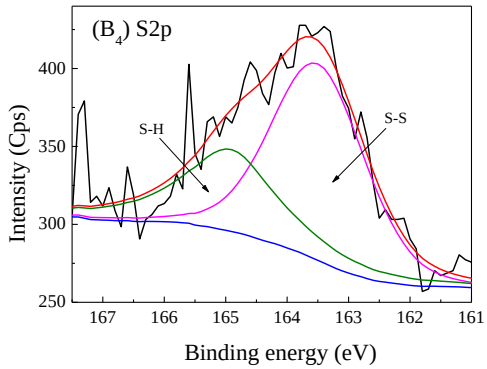
(B4) S2p
S-H
S-S
Intensity (Cps)
Binding energy (eV)

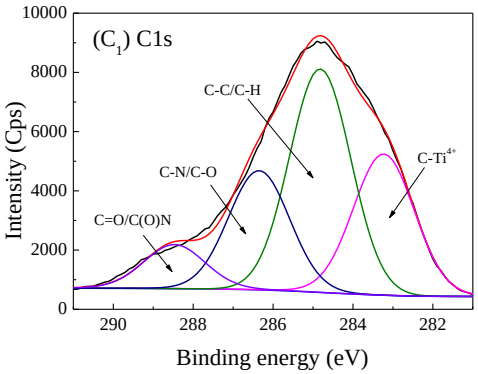
(C1) C1s
C-C/C-H
C-N/C-O
C=O/C(O)N
C-Ti4+
Intensity (Cps)
Binding energy (eV)

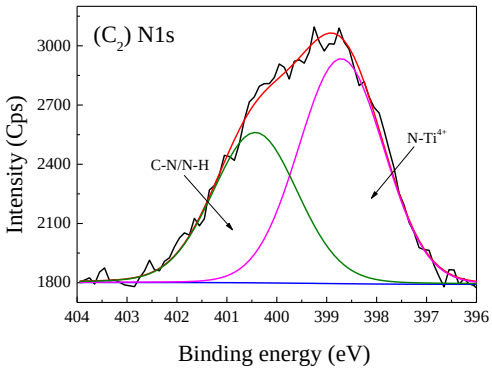
(C2) N1s
C-N/N-H
N-Ti4+
Intensity (Cps)
Binding energy (eV)

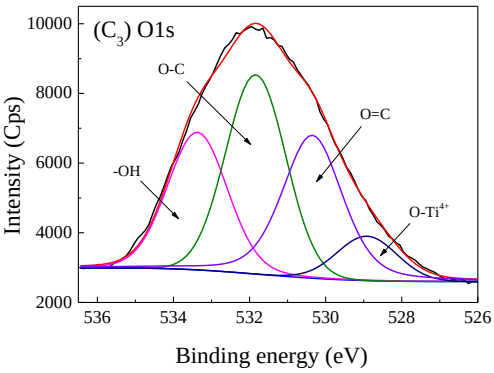
(C3) O1s
O-C
O=C
-OH
O-Ti4+
Intensity (Cps)
Binding energy (eV)

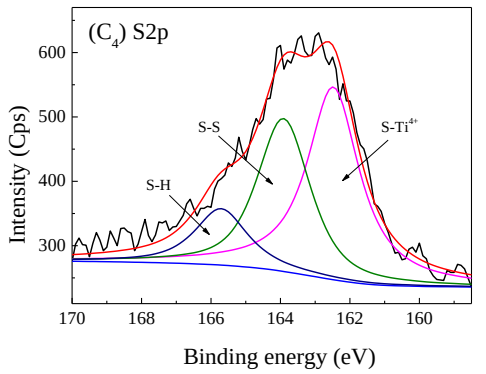
(C4) S2p
S-S
S-Ti4+
S-H
Intensity (Cps)
Binding energy (eV)

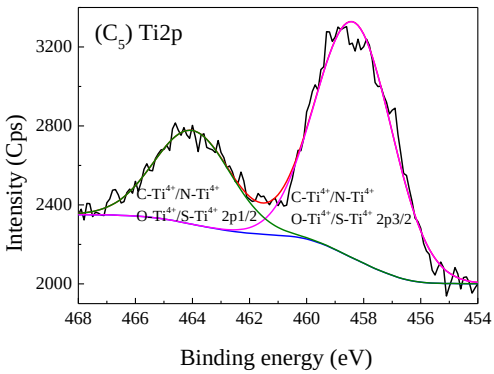
(C5) Ti2p
C-Ti4+/N-Ti4+
O-Ti4+/S-Ti4+ 2p1/2
C-Ti4+/N-Ti4+
O-Ti4+/S-Ti4+ 2p3/2
Intensity (Cps)
Binding energy (eV)

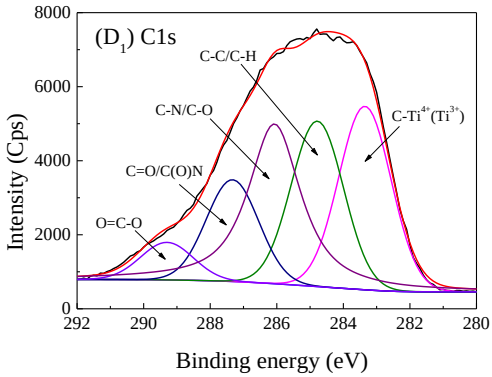
(D1) C1s
C-C/C-H
C-N/C-O
C=O/C(O)N
O=C-O
C-Ti4+(Ti3+)
Intensity (Cps)
Binding energy (eV)

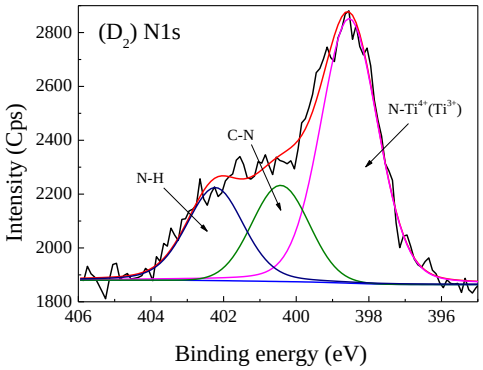
(D2) N1s
N-H
C-N
N-Ti4+(Ti3+)
Intensity (Cps)
Binding energy (eV)

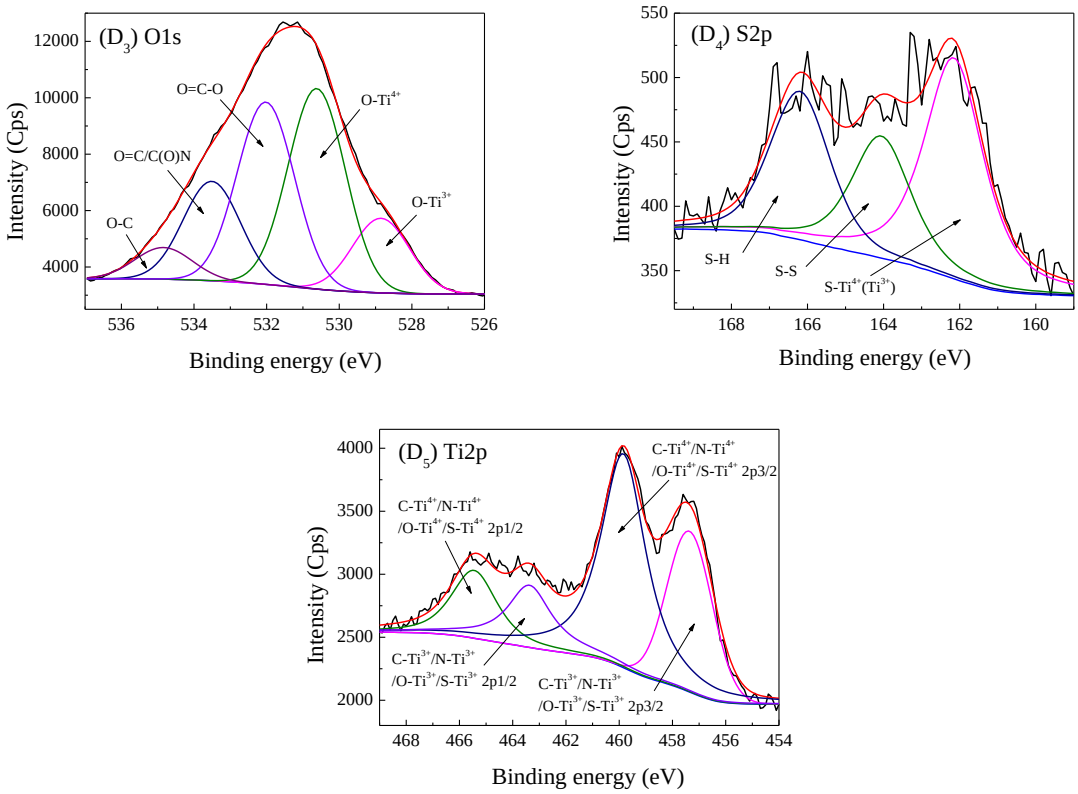

Figure 6. XPS spectra of wool fibers before and after treatments: (A) Survey spectra; (B_1) to (B_4) Original wool fiber; (C_1) to (C_5) for Scheme one; (D_1) to (D_5) for Scheme two.

Note: B_1, C_1,and D_1 for C_{1s} spectra; B_2, C_2,and D_2 for N_{1s} spectra; B_3, C_3, and D_3 for O_{1s} spectra; B_4, C_4,and D_4 for S_{2p} spectra; C_5 and D_5 for Ti_{2p} spectra

Table 1 XPS elemental analysis of wool fibers

Wool Fibers	Peak	Position BE (eV)	FWHM (eV)	Atomic Concentration (%)
Original	C1s	286.67	1.665	77.3
	N1s	397.9	2.03	1.02
	O1s	531.52	2.329	21.47
	S2p	162.04	2.333	0.21
Scheme one	C1s	284.39	2.13	71
	N1s	399.07	3.056	5.19
	O1s	530.74	2.753	20.91
	S2p	163.03	3.395	1.08
	Ti2p	463.91	3.549	1.82
Scheme two	C1s	288.97	2.227	67.71
	N1s	402.12	1.691	3.85
	O1s	532.85	3.677	25.39
	S2p	166.05	2.198	0.69

Ti2p	465.35	2.05	2.36

3.5. Structural changes of wool fibers

The two-dimensional X-ray diffraction images, X-ray diffraction patterns and orientation patterns of wool fibers before and after treatments are shown in Figure 7 below. It is evident from two-dimensional X-ray diffraction images as illustrated in Figure 7(a) that the molecule chains in the crystalline regions of the original wool fibers have preferred orientations at the angles of 0^o and 180^o parallel to the fiber orientation. The brightness of circular spots of their X-ray diffraction images shown in Figure 7 becomes dull and this indicates that the preferred orientations of the wool fibers obtained from the two schemes are weakened. These indicate that part of the α-helical keratin crystalline regions might have been transformed into irregular β-helical crystals[498] caused by the disordering effect of the swelling agents. Additionally, it is shown in Figure 7 that a series of diffraction rings are formed in the peripheries of the arc-shaped zones of the wool fibers obtained in the two schemes, this implies the existences of polycrystalline TiO_2 nanoparticles with the wool fibers. The crystallinity of wool fibers has decreased from 34.4% for the original wool fibers to 26.3% and 29.8% for fibers obtained from schemes one and two respectively.

It is noted in the diffraction patterns of the three wool fibers that, besides the characteristic diffraction peaks at around 9^o (the equatorial reflections of 0.98 nm for α-helix and β-sheet structure) and 20^o (the meridional reflections of 0.51 nm for α-helix structure and the equatorial reflections of 0.465 nm for β-sheet structure)[49] for wool fibers, a number of additional small diffraction peaks at 25°, 38°, 48°, 54°, 55°, 63°, and 75° in the XRD patterns are found for the wool fibers obtained from the two modification schemes. These additional diffraction peaks are attributed to the (101), (004), (200), (105), (211), (204), and (215) crystalline planes of anatase TiO_2 (JCPDS No.21-1272)[50] respectively. The corresponding orientation degrees of wool fibers are 0.72, 0.69, and 0.71 for the original wool fibers and modified wool fibers from schemes one and two respectively. So, the processes of swelling agent, infiltration of titanate

tetrabutyl and growth of TiO_2 result in a reduction of the crystallinity and slightly re-orientation of keratin molecules in modified wool fibers.

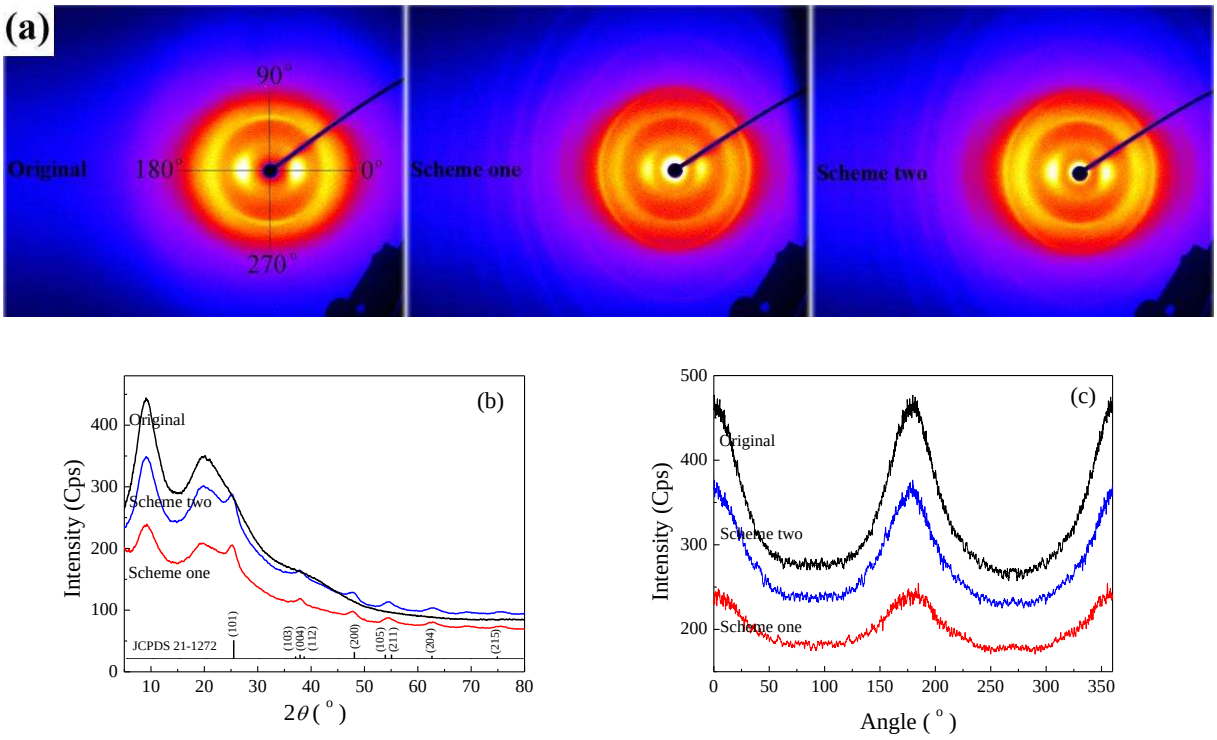

Figure 7. Two-dimensional X-ray diffraction images (a), X-ray diffraction patterns (b) and orientation patterns (c) of wool fibers before and after treatments

3.6. Light absorption capacities and photocatalytic properties

Light absorption and reflectance properties[25] of wool fibers before and after the two treatments are measured using diffused reflectance spectra (DRS) and depicted in Figure 8(a). The diffuse reflectance spectrum of the original wool fibers changes significantly after the two chemical modifications. For the wool fibers obtained from scheme one, their bandwidth to absorb UV rays is obviously broaden and the optical absorption edge is red-shifted to visible light regions. While both the original wool and the wool fibers obtained from scheme one have much smaller absorption capacity to visible light (in the range of wavelength between 380nm and 750 nm), it is particularly interesting to note that the wool fibers obtained from scheme two have markedly enhanced capacity of absorbing visible light as shown in the relationship[51] between $(\alpha hv)^2$ and the incident photon energy (hv) in Figure 8(b), where α is the absorption coefficient. The band gaps of the modified wool

fibers are 2.9 eV for scheme one and 2.8 eV for scheme two respectively, which are far smaller than 3.2 eV of theoretical value[52] of anatase TiO_2, as well as smaller than TiO_2 coated (3.2 eV) and N-doped TiO_2 coated (3.0 eV) wool fibers produced by hydrothermal method. This new energy levels in the band gap formed in the TiO_2 nanoparticles co-doped with carbon, nitrogen, oxygen, and sulphur in the wool fibers from scheme two leads to the production of more electron-hole pairs under the same visible-light irradiation, the TiO_2 nanoparticles might thus act as a trapping center for electrons and holes to reduce the recombination rate of charge carriers,[25] resulting in the higher photocatalytic activity.[53] Therefore, it is anticipated that the wool fibers obtained from scheme two will have excellent photocatalytic activities. When a TiO_2 nanoparticle (or an N- and S- doped TiO_2 nanoparticle) deposited on the wool fibers is exposed to light having the energy equivalent to or greater than the band gap energy of the Ti^{3+} ions on the surface of anatase TiO_2 nanoparticles (e.g., 3.2 eV for TiO_2 nanoparticles and 2.8 eV for the TiO_2-wool composites from the scheme two), electrons are excited from the valence band to the conduction band to produce electron-hole pairs on the TiO_2 surface. The photo-excited electrons are trapped by oxygen molecules to form superoxide radical anions ($O_2^{\cdot-}$) and lead to the reduction of Ti^{4+} cations to the Ti^{3+} state. In this process, the formation of oxygen vacancies is attained and O_2^- anions are oxidized by the photo-generated holes.[54] Meanwhile, the vacancy sites in TiO_2 are occupied by bound water molecules,[55] which is oxidized by the photo-generated holes to produce ($\cdot$OH) radicals, the TiO_2 nanoparticles thus are very reactive in the photocatalytic process generated using UV or visible light irradiation. It has been demonstrated that the RB degradation is mainly attributed to the participation of holes, $\cdot$OH and $O_2^{\cdot-}$ radicals,[56] as a result, RB dye molecules adsorbed on TiO_2 surface can be decomposed in the presence of those strong oxidant reagents.[57]

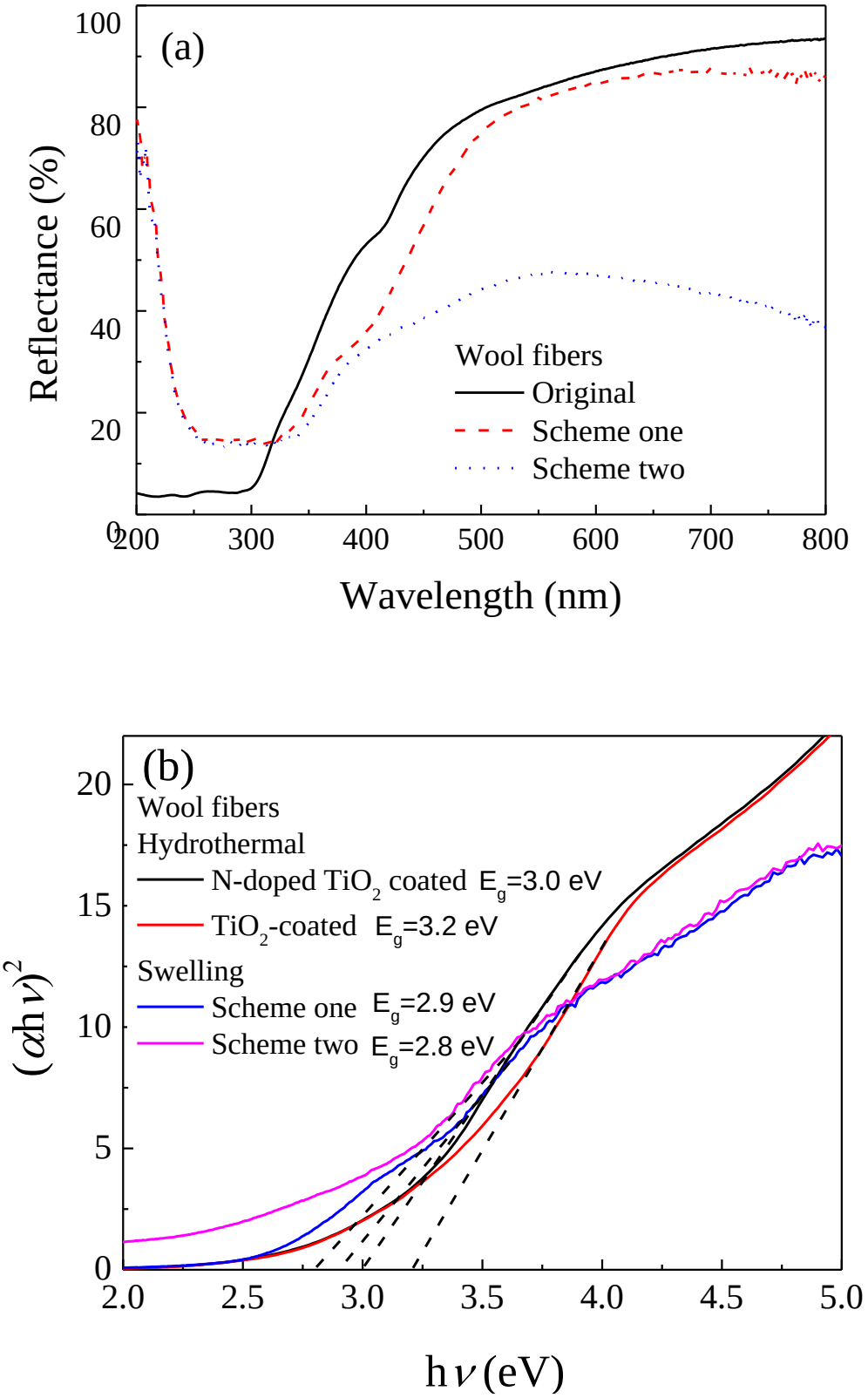

Figure 8. Diffuse reflectance curves of wool fibers before and after treatments

The photocatalytic degradation of RB dye solutions by using the resultant wool fibers under UV and visible

light illuminations can be represented as decolorization grade of RB dyes as shown in Figure 9. The decolorization grades of RB dyes by using all of the wool fibers including original wool, modified wool, and hydrothermally treated wool fibers increase with the increases of irradiation time under both UV and visible light irradiations (see Fig. 9). The photocatalytic degradation of RB dye solution by the original wool fibers under UV irradiation is primarily due to the degradation of dye molecules induced by UV rays and the adsorption of the RB dyes by the wool fibers.[58] Interestingly, the photocatalytic activity of the TiO_2 modified wool fibers obtained from scheme two (swollen by lithium bromide) and their decolorization grade to RB dyes are superior to the modified wool obtained from both scheme one (swollen by using formic acid) and hydrothermal process. The decolorization grades are 93.3% and 91.7% for the TiO_2-coated wool fibers obtained from scheme two and hydrothermal process respectively after 100 min of UV irradiation, and they are 94.4% and 92.6% for the two wools respectively after 60 min of irradiation by visible light. It is reported that the photodegradation of RB dyes follows approximately a first order kinetic model by the linear transforms $\ln(C_0/C) = f(t) = -kt$ (where k is the apparent photodegradation rate constant).[59] For the wool fibers obtained from scheme two, the photodegradation apparent rate constant, k, are 0.043 and 0.068 min^{-1} under UV and visible light irradiations respectively; they are greater than 0.024 and 0.050 min^{-1} for the TiO_2 coated wool fibers produced in the solely hydrothermal process under UV and visible light irradiations. The structural characteristics of the TiO_2 nanoparticles such as crystal phase, crystallinity, surface structure, surface area and total volume, might play an important role in RB dye degradation under present experimental condition.[25]

There are two main reasons for the superior photocatalytic effects of the TiO_2 nanoparticles coated on the wool fibers from scheme two. Firstly less energy is required for an electron transition because of the narrow energy band gap (2.8 eV) of Ti^{3+} in TiO_2 nanoparticles co-doped with carbon, nitrogen, oxygen and sulphur elements, and this leads to the enhanced visible light absorption; the existence of a large amount of TiO_2

nanoparticles co-doped with carbon, nitrogen, oxygen and sulphur elements in the wool fibers from scheme two in comparison with the absence of Ti^{3+} scavengers[60, 61] in the wool fiber from scheme one. Secondly, there are much greater amount of TiO_2 nanoparticles (estimated by TGA curves to be 10.6%) deposited on the wool fibers from scheme two in comparison with 3.7% of TiO_2 nanoparticles loaded on the wool fibers prepared by hydrothermal method. It is still unclear whether the TiO_2 nanoparticles formed inside the cortex of wool fibers obtained in scheme two contribute to the excellent photocatalysis effects, and further research on this effect is needed. The photocatalytic degradation of RB dye solutions by repeatedly using TiO_2 modified wool fibers obtained from scheme two was also performed at identical conditions. The decolorization grade of the wool fibers decreases with the increase of number of repeating times. After four times of repeated UV irradiation for 100 min and visible light irradiation for 60 min, the decolorization grades decrease to 63.8% and 64.7% respectively. The degraded RB solution is centrifuged for 15 min at a speed of 12000 rpm using a TG16-WS high-speed centrifuge (Hunan Xiang Yi Laboratory Instrument Development Co., Ltd, China). There is hardly any particle collected in the bottom of the solution. In addition, there is no Ti element shown in the ICP emission spectrometry of RB solution.

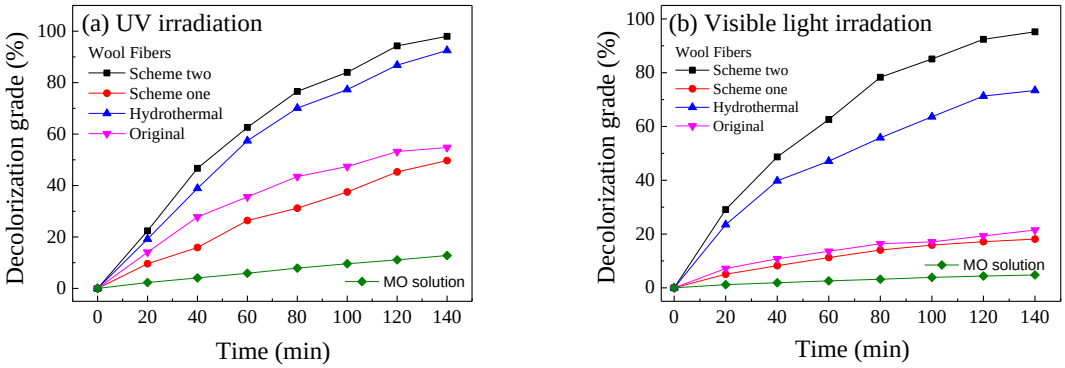

Figure 9. Decolorization grades of RB dye solutions against duration of irradiation for various wool fibers. (a) UV irradiation; (b) visible light irradiation

4. Conclusions

In this paper, a novel wool-TiO_2 nanoparticle composite material having TiO_2 nanoparticles formed both

inside the matrix between macrofibrils in cortical cells and on the surface of wool fibers is reported. The composite wool fibers have demonstrated highly photocatalytic properties with an extremely narrow band gap of 2.8 eV and can degrade rhodamine B (RB) dyes under both UV and visible light irradiations. This wool-TiO_2 nanoparticle composite material was developed via a process of three successive chemical treatments including wool swollen using lithium bromide, saturated with tetrabutyl titanate ethanol solution, and then hydrothermally treated in boiling water. It is discovered that non-crystallized TiO_2 nanoparticles (or nanoparticle aggregates) of the size of 50 nm formed in the matrix between macrofibrils inside the cortical cells of wool fibers swollen by lithium bromide and that crystallized anatase TiO_2 nanoparticles of the smallest energy band gap grafted on the surface of the fibers. It is found that elements of carbon, nitrogen, oxygen, and sulphur of wool fibers have reacted with the trivalent titanium of TiO_2 nanoparticles to form C-, N-, O- and S- doped TiO_2 nanoparticles, and that the chemical bonds formed between the as-synthesized TiO_2 nanoparticles and the wool fibers include C-Ti^{4+}(Ti^{3+}), N-Ti^{4+}(Ti^{3+}), O-Ti^{3+}, and S-Ti^{4+}(Ti^{3+}) bonds. The wool fibers obtained via this sequential treatment approaches have markedly improved photocatalytic efficiency in comparison with (N-doped) TiO_2 coated wool fibers in degrading RB dyes under both UV and visible light illuminations which is attributed to their enhanced visible light absorption capability. However, it is unclear whether the excellent photocatalytic degradation effect is linked with the TiO_2 nanoparticles formed inside the wool cortex. In contrast, TiO_2 modified wool fibers swollen by using formic acid have poorer photoactivity and photocatalytic degradation effect on RB dye solutions and no TiO_2 nanoparticles were found inside this wool fiber while the tetrabutyl titanate solution was confirmed to have penetrated into the cortex matrix, this might be due to the elimination of trivalent titanium between TiO_2 nanoparticles and the wool fibers.

Notes

The authors declare no competing financial interest.

Acknowledgments

The authors acknowledge the supports from the Sanqin Scholar Foundation (2017) and Hundred Talent Programme of Shaanxi Province, and the China Scholarship Council.

References

[1] Popescu C and Hocker H 2007 Chem. Soc. Rev. **36** 1282

[2] Naylor G R S 2010 Tex. Res. J. **80** 537

[3] Liu H L and Yu W D 2007 J. Appl. Polym. Sci. **104** 816

[4] Yuan J G, Wang Q, Fan X R and Wang P 2010 Tex. Res. J. **80** 1898

[5] McNeil S J, Sunderland M R and Leighs S J 2017 Appl. Catal. A–Gen. **541** 120

[6] Zhang L X, Liu P and Su Z X 2006 Mater. Chem. Phys. **98** 111

[7] Bottcher H, Mahltig B, Sarsour J and Stegmaier T 2010 J. Sol-Gel Sci. Techn. **55** 177

[8] Sobczyk-Guzenda A, Szymanowski H, Jakubowski W, Basiska A, Kowalski J and Gazicki-Lipman M 2013 Surf. Coat. Tech. **217** 51

[9] Galkina O L, Sycheva A, Blagodatskiy A, Kaptay G, Katanaev V L, Seisenbaeva G A, Kessler V G and Agafonov A V 2014 Surf. Coat. Tech. **253** 171

[10] Tomsic B, Jovanovski V, Orel B, Mihelcic M, Kovac J, Francetic V and Simoncic B 2015 Cellulose **22** 3441

[11] Vaez M, Moghaddam A Z, Mahmoodi N M and Alijani S 2012 Process Saf. Environ. **90** 56

[12] Subianto H, Nuryadin B W, Khairurrijal, Mahfudz H, Dananjaya N and Abdullah M 2013 J. Mater. Cycles Waste **15** 210

[13] Wiener J, Shahidi S and Goba M M 2013 Opt. Laser Technol. **45** 147

[14] Kramer A, Kunz C, Graf S and Muller F A 2015 Appl. Surf. Sci. **353** 1046

[15] Johnston J H and Lucas K A 2011 Gold Bull. **44** 85

[16] Harris M, Mizell L R and Fourt L 1942 Ind. Eng. Chem. **34** 833

[17] Sookne A M and Harris M 1937 J. Res. Natl. Bur. Stand. **19** 535

[18] Hearle J W S 2007 J. Mater. Sci. **42** 8010

[19] Zhang H, Yang Z W, Zhang X T and Mao N T 2014 Chem. Eng. J. **254** 106

[20] Montazer M and Seifollahzadeh S 2011 Photochem. Photobiol. **87** 877

[21] Behzadnia A, Montazer M, Mahmoudi Rad M 2016 Photochem. Photobiol. **92** 76

[22] Zhang H and Zhu H 2012 J. Tex. I. **103** 1108

[23] Zhang H, Xu J and Zhang X T 2015 J. Nat. Fibers **12** 518

[24] Zhang H, Yan H Y and Mao N 2014 Ind. Eng. Chem. Res. **53** 2030

[25] Yadav S and Jaiswar G 2017 J. Chin. Chem. Soc. **64** 103

[26] Segal L, Creely J J, Martin Jr A E and Conrad C M 1959 Tex. Res. J. **29** 786

[27] Bohn A, Fink H-P, Ganster J and Pinnow M 2000 Macromol. Chem. Phys. **201** 1913

[28] Mills A and Wang J 1999 J. Photoch. Photobio. A. **127** 123

[29] Galagan, Y. & Su, W. F. Reversible photoreduction of methylene blue in acrylate media containing benzyl dimethyl ketal. J. Photochem. Photobiol. A **195**, 378–383 (2008).

[30] Liu, B., Wen, L., Nakata, K., Zhao, X., Liu, S., Ochiai, T., Murakami, T. and Fujishima, A. (2012), Polymeric Adsorption of Methylene Blue in TiO_2 Colloids—Highly Sensitive Thermochromism and Selective Photocatalysis. Chem. Eur. J., **18**: 12705-12711. doi:10.1002/chem.201200178

[31] Wei Y J, Li K A and Tong S Y. 1996 Chem. Res. Chinese U. **17**, 1687

[32] Hu X F, Mohamood T, Ma W H, Chen C C and Zhao J C 2006 J. Phys. Chem. B **110**, 26012

[33] Wang P, Cheng M M and Zhang Z H 2014 J. Saudi Chem. Soc. **18**, 308

[34] Liu C, Sun T, Wu L, Liang J Y, Huang Q J, Chen J and Hou W H 2015 Appl. Catal. B–Environ. **S170-171**, 17

[35] An X H, Meng G W, Zhang M G, Tian Y T, Sun S H and Zhang L D 2006 Mater. Lett. **60** 2586

[36] Richardson M J and Johnston J H 2007 J. Colloid Interf. Sci. **310** 425

[37] Ma W, Wen F, Xie D, Leng Y X and Mu Z L 2014 J. Adv. Ceram. **3** 49

[38] Molina R, Espinos J P, Yubero F, Erra P and Gonzalez-Elipe A R 2005 Appl. Surf. Sci. **252** 1417

[39] Wang X H, Li Y M, Liu S M and Zhang L 2016 Nanomaterials **6** 40

[40] Meade S J, Dyer1 J M, Caldwell J P and Bryson W G 2008 Tex. Res. J. **78** 943

[41] Li F, Han T H, Wang H G, Zheng X M, Wan J M and Ni B K 2017 J. mater. Res. **32** 1563

[42] Khan M M, Ansari S A, Pradhan D, Ansari M O, Han D H, Lee J and Cho M H 2014 J. Mater. Chem. A. **2** 637.

[43] Mori1 M and Inagaki N 2006 Tex. Res. J. **76** 687

[44] Arman S Y, Omidvar H, Tabaian S H, Sajjadnejad M, Fouladvand Sh and Afshar Sh 2014 Surf. Coat. Tech. **251** 162

[45] Han T R, Chen Y J, Tian G H, Zhou W, Xiao Y T, Li J X and Fu H G 2016 Sci. China Mater. **59** 1003

[46] Xiong L B, Li J L, Yang B and Yu Y 2012 J. Nanomater. **2012** 208

[47] Tan H Q, Zhao Z, Zhu W B, Coker E N, Li B S, Zheng M, Yu W X, Fan H Y and Sun Z C 2014 ACS Appl. Mater. Inter. **6** 19184

[48] Xiao X L and Hu J L 2016 Int. J. Chem. Eng. **2016** 1

[49] Niu M, Liu X G, Dai J M, Hou W S, Wei L Q and Xu B S 2012 Spectrochim. Acta Mol. Biomol. Spectrosc. **86** 289

[50] Yang W G, Wang Y L and Shi W M 2012 CrystEngComm **14** 230

[51] Reyes-Coronado D, Rodriguez-Gattorno G, Espinosa-Pesqueira M E, Cab C, de Coss R and Oskam G

2008 Nanotechnology **19** 145605

[52] Li W, Liu C, Zhou Y X, Bai Y, Feng X, Yang Z H, Lu L H, Lu X H and Chan K Y 2008 J. Phys. Chem. C **112** 20539

[53] Ketteler G, Yamamoto S, Bluhm H, Andersson K, Starr D E, Ogletree F D, Ogasawara H, Nilsson A and Salmeron M 2007 J. Phys. Chem. C **111** 8278

[54] Qi D Y, Xing M Y and Zhang J L 2014 J. Phys. Chem. C **118** 7329

[55] Bharati B, Sonkar A K, Singh N, Dash D and Rath C 2017 Mater. Res. Express **4** 085503

[56] Zheng X Z, Li D Z, Li X F, Yu L H, Wang P, Zhang X Y, Fang J L, Shao Y and Zheng Y 2014 Phys. Chem. Chem. Phys. **16** 15299

[57] Hsiao Y C, Wu T F, Wang Y S, Hu C C and Huang C 2014 Appl. Catal. B–Environ. **S148-1449** 250

[58] Pielesz A 2004 J. Appl. Polym. Sci. **91** 2629

[59] Abdel-Monem Y K 2016 J. Mater. Sci. Mater. Electron. **27** 5723

[60] Hou H M, Miyafuji H and Saka S 2006 J. Mater. Sci. **41** 8295

[61] Jun T H, Lee K S and Song H S 2012 Thin Solid Films **5210** 2609